Investigation of the dynamics of a Capillary Pumped Loop assisted with a mechanical pump: Influence of pump location

Marie Lévêque, Sébastien Dutour

Investigation of the dynamics of a Capillary Pumped Loop assisted with a mechanical pump: influence of pump location.

Marie Levêque[a,b], Sébastien Dutour[a,*]

[a] *University of Toulouse, UPS, INPT, CNRS, LAPLACE, 118 route de Narbonne, F-31062 Toulouse cedex 9, France.*
[b] *IRT-saint Exupéry, 118, route de Narbonne - CS 44248, 31432 Toulouse cedex 4, France*

Abstract

Capillary driven two-phase loops are promising solutions for cooling high power electronic devices. A significant upgrade of the operating conditions can be achieved by a small mechanical pump assistance removing the pumping limit inherent to the evaporator porous wick. However, in this couplings, the key issue is to maintain a steady vaporization regime in the evaporator. In the present study, the dynamics of a Capillary Pumped Loop assisted with a centrifugal pump is investigated with both experiments and modeling efforts. The results have revealed (i) that changing the pump location can deteriorate the system robustness with 5 times larger ($2.25\,kPa$) evaporator pressure deviations and (ii) the appearance of a system bifurcation to undamped oscillations at high heat load. A theoretical analysis was performed in frequency domain. It has shown that the loop dynamics is affected by an unexpected transient positive feedback between the pump and the condenser. It has also shown that the loop robustness could be enhanced within a significant range of heat load by a suitable improvement of the condenser efficiency.

Keywords: Capillary Pumped Loop, mechanical pumping, transient modeling, electronic cooling

Nomenclature

Symbol, definition, SI units

A	surface area m^2
a	first pump parameter Pa/rpm^2
b	second pump parameter $Pa\,s/(kg\,rpm)$
D	diameter, m
G	thermal conductance, W/K
g	gravity, m/s^2
h	heat transfer coefficient, $W/K/m^2$
ΔH_{vap}	enthalpy of vaporization, J/kg
K_p	proportional coefficient, rpm/Pa
L	length, m
m	mass flow rate, kg/s
MC	evaporator total capacitance J/K
Q	heat load, W
w	rotational speed, rpm
Z	height above the condenser position, m

Greek symbols

α	mean vapor fraction at the condenser
ω	frequency, rad/s
ρ	density, kg/m^3
τ_I	control integral coefficient, s

Subscripts

2φ	two-phase condensation zone
C	condenser
cap	capillary
Ev	evaporator
i	inner
in	inlet
ℓ	liquid
$\ell\ell$	liquid line
o	outer
out	outlet
p	peak
R	reservoir
sat	saturation
set	set point
v	vapor
w	wall

1. Introduction

Two-phase loop systems are promising solutions for cooling high heat flux density and high power electronic devices. In particular, capillary two-phase loops such as Capillary Pumped Loop (CPL) and Loop Heat Pipe (LHP) permit to transport high amount of heat on several meters [1]. The performance is mainly due to the evaporator which simultaneously ensures heat dissipation by vaporization within a porous wick and fluid circulation by capillary pumping. As long as the vaporization regime is maintained in the wick, the heat transfer efficiency

*corresponding author
Email address: sebastien.dutour@laplace.univ-tlse.fr (Sébastien Dutour)

is high and robust. However, the mean pore diameter imposes a maximum pressure head called the capillary limit which is about tens of kPa with the most suitable fluids (ammonia, alcohol). Another limit called the boiling limit exists when vapor nucleation begins upstream the interface stopping the liquid supplying at the evaporator inlet. The coupling of a capillary two-phase loop with a small mechanical pump is a way to overcome these limits and more generally, to largely improve the operating conditions.

Schweickart et al. [2] used a controlled volumetric pump placed downstream the reservoir in order to increase the transport length of a CPL with eight parallel evaporators for space application. The results were limited by the evaporator flooding due to some difficulties to control the fluid circulation. Another approach was initially proposed by Park et al. [3], Crepinsek and Park [4] and Bejarano and Park [5] with the objective to transfer high heat flux density. Here, the evaporator is located on a parallel branch starting from the pump outlet and ending within the reservoir. The flow distribution depends on both capillary regime in the evaporator branch and pump action in the main branch. In the most recent work, Lee and Park [6] greatly improved the control of the vaporization regime and a heat density of 227 W/cm^2 was reached. The effect of fluid charging in the loop was investigated by Jiang et al. [7] on a similar device [8]. Zhang et al. [9] used a micro centrifugal pump to evacuate a heat flux density of 36.35 W/cm^2 with ammonia and a mini-LHP evaporator. Another configuration was proposed by Setyawan et al. [10], with the objective to avoid the transient evaporator dry-out.

An overview of the studies cited above shows that the key issue is to maintain the vaporization regime in the evaporator as the mechanical pump modifies the fluid circulation. An original pump assistance of a CPL has thus been proposed (Levêque et al. [11]) and we have shown that the hybrid CPL (HCPL) acts as it would in a simple capillary-driven regime preserving the evaporator thermal efficiency. The total loop pressure drop has reached more than 60 kPa i.e. more than 6 times the evaporator capillary limit without significant dry-out. Compared to flow boiling loop, the capillary evaporator still operates with "negative" pressure drop (inlet minus outlet pressure). As a consequence, the pump power is incomparably small in hybrid capillary systems.

The principle of the approach is shown in figure 1. A centrifugal pump is located downstream the reservoir (configuration called HCPL-RO for "Reservoir Outlet"). The pressure losses in the evaporator grooves and the vapor line (from 1 to 3), in the liquid line and condenser until the reservoir inlet (3 to 5) are balanced by both the centrifugal pump head (from 5 to 5') and the capillary pressure (from 6 to 1). It is then possible to maintain the capillary pressure lower than its limit by controlling the pump head. However, the proposed HCPL-RO configuration is only suitable for a CPL since, by construction, the LHP evaporator includes the reservoir. Moreover, the influence of the pump location in the HCPL configuration has not been studied so far. Actually, locating the pump at the reservoir inlet appears to be a delicate situation for the system control: the liquid line hydrodynamics is stronger because of the liquid

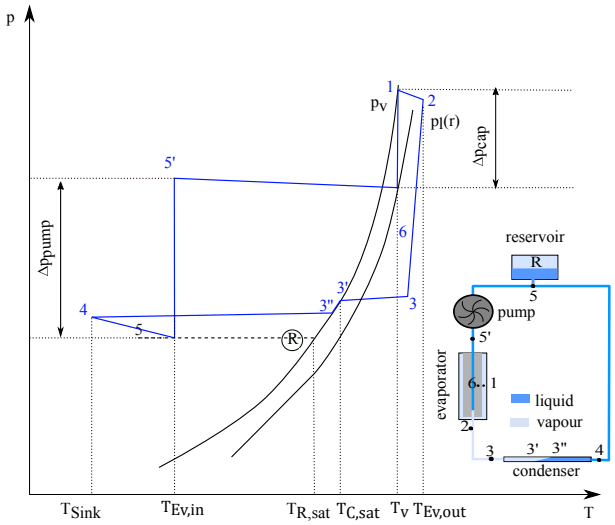

Figure 1: HCPL-RO operating cycle.

discharge between the condenser and the reservoir. This could drastically affect the ability to control the hybrid system. Moreover, as shown in figure 2, the pressure-temperature cycle is also significantly modified with the pump position.

An investigation of the HCPL dynamics is proposed in this study in order to establish the influence of the pump location. Some new tests are performed on a CPL assisted with a pump located at the reservoir inlet (HCPL-RI). The response to heat load steps is compared to the HCPL-RO results. Differences in the systems robustness and thermal characteristics are established. Then, a model is proposed in order to identify the fundamental mechanisms ruling out the HCPL dynamics and stability for both pump configurations. Finally, it also allows to determine how the HCPL robustness can be improved.

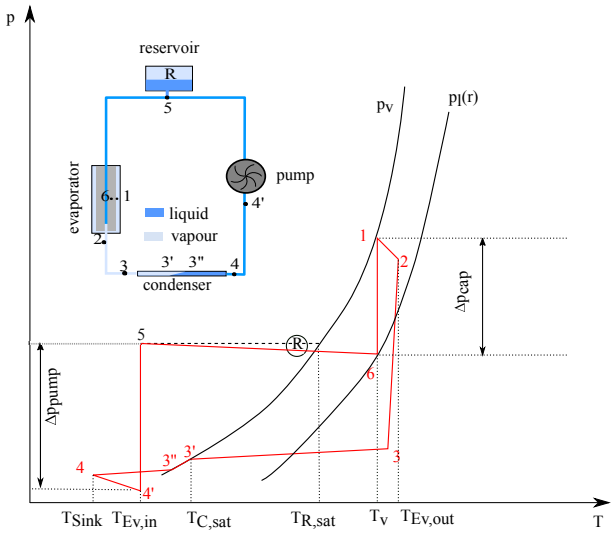

Figure 2: HCPL-RI operating cycle.

2. Experimental set-up

2.1. HCPL set-up

The HCPL devices are composed of four main elements : a vertical flat capillary evaporator, a thermally regulated reser-

voir, a counter-flow double pipe condenser and a centrifugal pump (figure 3). The working fluid is methanol. Both evaporator and reservoir were initially developed for power electronics cooling. The major geometrical features are provided in table 1.

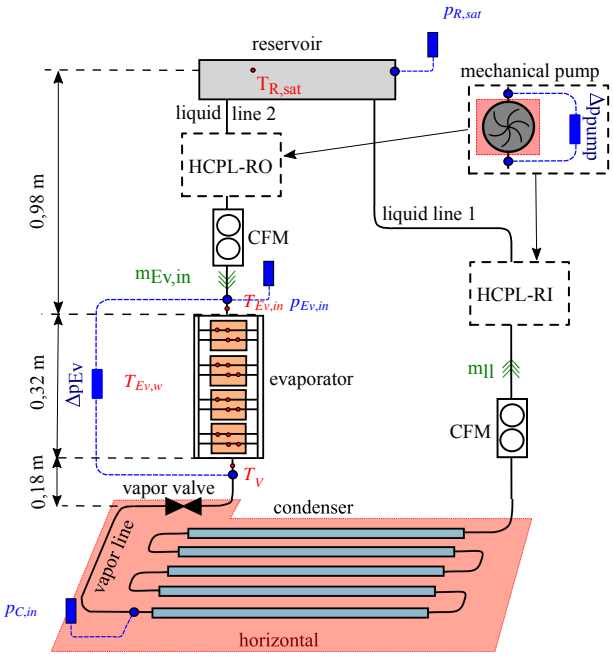

Figure 3: Schematic of the HCPL with instrumentation. CFM: Coriolis Flow Meter.

The evaporator porous wick is made of sintered nickel powder. Trapezoidal vapor grooves are directly machined on its surface. Similar evaporators were studied by Ayel et al. [12], Dupont et al. [13] and more recently by Accorinti et al. [14] who focused on the evaporator thermal performance. Power is applied to both sides of the evaporator through 2×4 copper diffusive blocks each including three cylindrical cartridge heaters. A mechanical apparatus using springs controls the strength and the uniformity of the contact between the blocks and the evaporator wall. A detailed description is available in Kaled et al. [15]. The heat leak with ambiant was previously estimated by a uniform heating of the evaporator wall when high vacuum was made in the loop: it reached $[76 \pm 2\,W, 89 \pm 3\,W]$ when the evaporator temperature was included in $[65°\,C, 80°\,C]$ with an ambiance at $22°C$.

The condenser is made of a double coaxial glass tube. A transparent silicon oil coolant circulates in the external tube. Its thermal regulation is performed by an external cooling system. Compared to the use of a classical metallic tube, this choice reduces the condenser overhall heat transfer but it was assumed in order to visualize the condensation zone pattern. Hence, the position of the condensation front is followed with a high speed frequency camera. The reservoir temperature is regulated to a set point using a heater associated with a PID controller. The heater balances the heat losses with the cold liquid flowing in the lower part of the reservoir.

The pump differential pressure can reach $60\,kPa$ for a flow rate up to $10\,g/s$. The impeller rotational speed ranges from $4,000\,rpm$ to $30,000\,rpm$ with a maximal speed increase of $2,000\,rpm$ per second. The impeller is located in a sealed casing and it is driven by magnetic force. The pump performance curve is available in Levêque et al. [11]. The pump power is proportional to the rotational speed. The operating power range is $[1.5\,W - 13\,W]$. The heat dissipated by the pump into the cycle is thus negligible.

Components	Dimensions
Evaporator	$320 \times 81 \times 20\,mm$
	wall thickness: $1\,mm$
Wick	$283 \times 68 \times 16\,mm$
	mean pore diameter: $6.8\,\mu m$
	permeability: $6.53\ 10^{-13}\,m^2$
	porosity: 73%
Vapor line	i.d.: $12\,mm$
	length: $3.3\,m$
Condenser	i.d.: $12\,mm$
	length: $7.2\,m$
Liquid line 1	i.d.: $6\,mm$
(reservoir inlet)	length: $1.5\,m$
Reservoir	volume: $2\ 10^{-3}\,m^3$
Liquid line 2	i.d.: $10\,mm$
(evaporator inlet)	length: $1\,m$
Pump	volume: $18 \times 9 \times 4\,cm$
	mass: $650\,g$
Fluid	mass: $1.5\,kg$

Table 1: HCPL main features.

Figure 3 shows the instrumentation implemented on the HCPL. K-type thermocouples measure the temperature on external surfaces of pipes along lines and in $0.6\,mm$ diameter grooves machined in the evaporator wall. In order to control and follow the pressure gain and losses along lines and components, pressure transducers measure the pressure difference between the fluid entrance and exit of the evaporator, the centrifugal pump and lines. An absolute $0 - 3\,bar$ pressure transducer is placed on the upper part of the reservoir. Associated with a $2\,mm$ diameter platinum probe, these measurements allow to detect a potential appearance of non-condensable gases. The liquid mass flow rate at the inlet and at the outlet of the reservoir are measured with Coriolis flow-meters. Data acquisition is at least carried out every second.

A thermocouples calibration was performed: the thermocouples were placed in a copper thermal mass immersed in a dedicated thermostatic bath. The electronic compensation was performed by the acquisition system at the reference junction. The thermal mass temperature was monitored using a Pt100 probe calibrated by an approved center (National Calibration Instruments) with an uncertainty of $0.015°C$. The expanded uncertainty obtained after calibration is $0.1°C$ in the entire operating range with a coverage factor $k = 2$. Other measurement uncertainties are given in table B.2.

2.2. *Evaporator differential pressure control scheme*

A pump control scheme is used with the objective to maintain the capillary driven pumping even when the total pressure drop in the loop, Δp_{loop}, exceeds the capillary limit [11]. When the

flow inertia is weak, this pressure difference can be found as the sum of the differential pressure at the evaporator Δp_{Ev} and at the pump Δp_{pump}:

$$\Delta p_{loop} = \Delta p_{Ev} + \Delta p_{pump} \quad (1)$$

Then, comparing this pressure drop to a set point for the evaporator pressure $\Delta p_{Ev,set}$, two regimes can be achieved:

- when $\Delta p_{loop} \geq \Delta p_{Ev,set}$, the mechanical pump is started and an automatic control regulates the rotational speed such as Δp_{Ev} remains as close as possible to the set point: the HCPL reaches the pump-assisted capillary-driven (PACD) regime.
- when $\Delta p_{loop} < \Delta p_{Ev,set}$, the mechanical pump is switched off and then it acts as a passive component: the HCPL operates in a simple capillary-driven (CD) regime.

Under the PACD regime, the controller used to regulate the differential pressure at the evaporator is a proportional-integral (PI) controller. Values of both constants K_P and τ_I were experimentally adjusted maximizing the system response for both architectures.

2.3. Experimental procedure

In the following experiments, a valve located on the vapor line is used in order to test the system with a maximum loop pressure drop. The objective is to demonstrate that both HCPL can operate beyond the capillary limit. This was experimentally found to be close to $9\,kPa$. The flow resistance in the loop is mainly produced by the valve plug such that $\Delta p_{valve} \approx \Delta p_{pump}$.

The reservoir temperature and the coolant temperature were respectively maintained to $65°C$ and $25°C$. $\Delta p_{Ev,set}$ is set at $5.75\,kPa$. Then, heat load steps were uniformly applied on both sides of the evaporator with a moderate step amplitude of $0.2\,kW$. The maximum power input of $1.6\,kW$ is imposed by the condenser.

3. Experimental results and analysis

A global overview of the experimental results is respectively given in figure 4 for the HCPL-RO and in figure 5 for the HCPL-RI. In the following discussion, we will focus on some of them with the objective to compare the system robustness and the thermal performance.

3.1. Comparison of robustness

In robustness, we mean the system ability to relax to a $\Delta p_{Ev,set}$ set point with reduced Δp_{Ev} overshoot and short time response when a heat load change is made at the evaporator.

The results shows first that both configurations are able to operate beyond the capillary limit. However, the maximum power cannot be applied for the HCPL-RI because of the appearance of some large amplitude oscillations at $t \simeq 190\,min$. The system has to be stopped after $20\,min$ because the oscillations amplitude continues to increase and finally, it could damage the pump. Thus, Δp_{loop} is here limited to $30\,kPa$ when the pump is placed at the reservoir inlet.

Moreover, focusing on the Δp_{Ev} overshoot consecutive to the heat load steps $0.6\,kW$ to $0.8\,kW$ and $0.8\,kW$ to $1\,kW$, provided in figure 6 with a more appropriate scale, the difference between the overshoot amplitude of both architectures is obvious. The amplitude of HCPL-RI overshoots are respectively 2.7 and 4.5 times higher than for HCPL-RO indicating a general deterioration of the HCPL robustness when the pump is placed at the reservoir inlet. On top of that, when the heat load increases, the overshoot amplitude decreases from $0.65\,kPa$ to $0.5\,kPa$ for the HCPL-RO: a high heat flux tends to stabilize the system. Conversely, it increases from $1.75\,kPa$ to $2.25\,kPa$ with the heat flux for the HCPL-RI.

The liquid dynamics in the line between the condenser and the reservoir is also greatly influenced by the pump location: the flow rate m_{ll} overshoot on figures 4.b and 5.b is three to six times higher for the HCPL-RI. This overshoot amplifications shows the impact of the pump on the reservoir-condenser coupling and on the liquid redistribution. The feedback between the pump and the condenser seems then to be important under this configuration and has to be further investigate.

A magnification of the oscillations between $t = 190\,min$ and $t = 220\,min$ is provided in figure 7. The time-period is about $4-5\,min$. The pressure amplitude grows from $15\,kPa$ to $20\,kPa$ in $30\,min$ around the mean value of $30\,kPa$. These oscillations follow the flow rate overshoot occurring in the liquid line at $t = 194\,min$. The sub-cooled liquid at $25°C$ fills the reservoir and causes the reservoir temperature $T_{R,sat}$ variations despite the external control (figure 7.c). This mass redistribution between the condenser and the reservoir also leads to a significant variation of the condenser saturation temperature and pressure. The pressure decrease leads to a flow inversion in the liquid line. As a check valve is installed on the liquid line, the fluid cannot comes from the reservoir to refill the condenser.

However, it is noticeable that the flow rate at the inlet of the evaporator is nearly not influenced, while the evaporator pressure difference experiences some oscillations of moderate amplitude ($2\,kPa$). Nevertheless, the capillary evaporator is robust enough to never reached its limits (no vapor percolation or flooding of the evaporator). Then, even if the evaporator undergoes the oscillations, it doesn't seem to play a major role in their apparition and amplification.

The instability of the HCPL-RI are damaging for the system, and further investigations are then needed to determine the multiple mechanisms at the origin and a way to stabilize this configuration. In order to fulfill this goal, some modeling efforts are presented in section 4.

3.2. Differences in thermal performance

Multiple criteria can be used to characterize a two-phase loop thermal performance. In this subsection, we focus on (i) the loop capacity to have a low temperature variation at the evaporator vs the heat load range, (ii) the thermal performance at the condenser and (iii) the efficiency of reservoir/evaporator coupling to avoid the boiling limit at the evaporator inlet. These aspects will be compared between each architectures.

As previously mentioned, the pump location has a high impact on the pressure range of the operating cycle (see figures 1

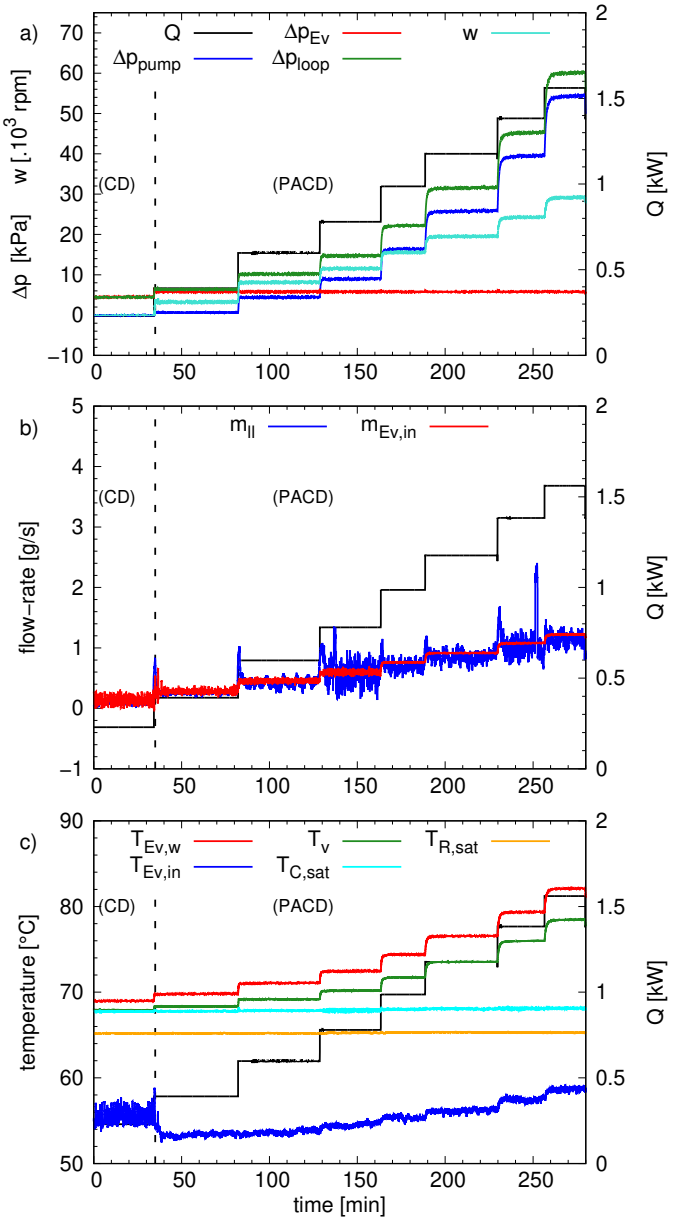

Figure 4: HCPL-RO response to moderate heat load steps: pressure differences and pump rotational speed a), mass flow rate b) and temperature variation c).

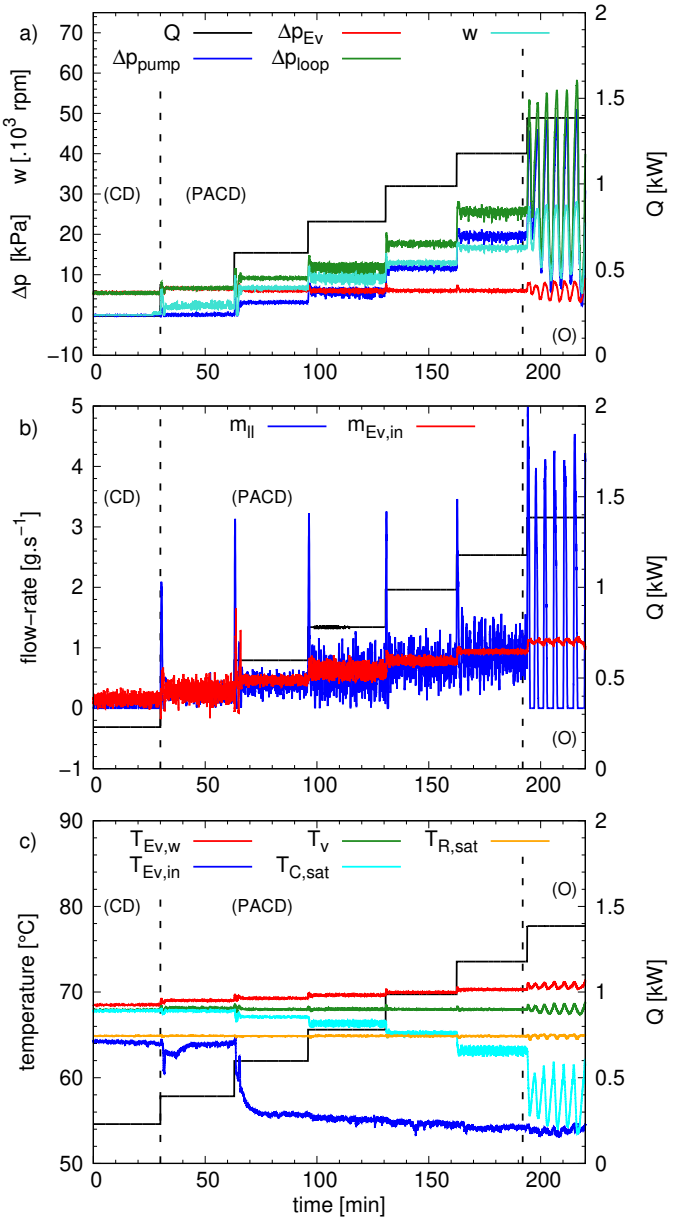

Figure 5: HCPL-RI response to moderate heat load steps: pressure differences and pump rotational speed a), mass flow rate b) and temperature variation c).

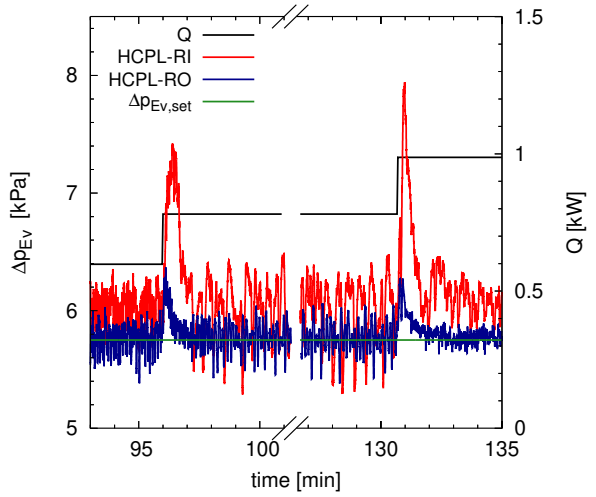

Figure 6: Comparison of the evaporator pressure difference consecutive to some representative heat load steps.

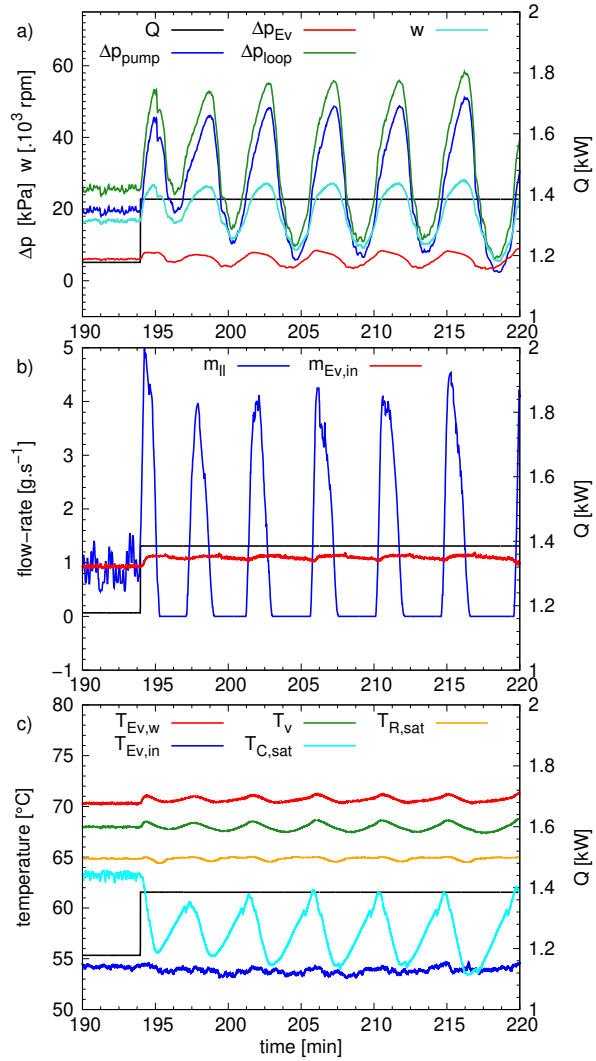

Figure 7: Magnification on oscillations : pressure differences and pump rotational speed a), mass flow rate b) and temperature variation c).

and 2). As a consequence, it has a significant influence on the saturation temperatures in the loop. The saturation temperature in the reservoir is fixed but, the pump pressure action will lead to an increase of the vaporization temperature for the HCPL-RO while it will decrease the condensation temperature for the HCPL-RI. This is confirmed in figures 4.c and 5.c. An overview of the evaporator wall temperatures at steady-state is also given on figure 8. The HCPL-RI has the interesting ability to maintain the vapor temperature almost constant with the heat load. Actually, it only varies with the small pressures losses in the line between the reservoir and the evaporator. For the HCPL-RO, T_v increases with the pump pressure head i.e. with the loop pressure losses. At $1.2\,kW$, the pressure head is $\sim 20\,kPa$. With a saturation pressure sensitivity of $4\,kPa$ by degree, it is consistent with the observed $6\,K$ evaporator temperature difference between both configurations.

The HCPL-RO evaporator temperature increase can be related to the HCPL-RI temperature decrease in the condenser: a corresponding temperature decrease of about $6\,K$ is also achieved at $1.2\,kW$ within the condenser (figure 5.c). However, this leads to another effect: a smaller temperature difference between the condensation temperature and the heat sink leads to a decrease of the heat transfer density and consequently to a modification of the condensation length. Figure 9 compares the mean condensation length obtained by vizualisation. The end of the condensation zone was determined as a function of time by video tracking. At steady-state, this provided a periodic signal due to permanent flow plugging (interface instability) with a period δt included in $[1\,s, 10\,s]$. The time duration selected for averaging was $10 \times \delta t$ and included 10 frames by second. The error bars show the maximum and minimum positions i.e the signal amplitude. Actually, it is observed that the HCPL-RI condensation zone becomes significantly greater at high heat load. The increase reaches about 25 ± 11 % at $1.2\,kW$ which is consistent to the corresponding 15% decrease of the temperature difference. Finally, these results shows that a special attention to the condenser performance must be given for the HCPL-RI configuration.

The boiling limit highly depends of the liquid sub-cooling at the evaporator inlet i.e. $T_{Ev,in} - T_{Ev,in,sat}$. Figure 10 gives this sub-cooling at steady-state for both configurations and for different heat loads. The error bars provide the uncertainty determined using table B.2. As the saturation temperature at the inlet of the evaporator varies considerably for the HCPL-RO, the liquid sub-cooling is greatly increased and finally, this configuration favorably prevents the evaporator from the boiling limit. Otherwise, the sub-cooling is significantly smaller at low heat load revealing the existence of both liquid and vapor at the evaporator inlet. The boiling point is actually reached inside the wick at $0.2\,kW$ and $0.4\,kW$ but the vapor amount is not high enough to stop the wick liquid supply.

4. Modeling and analysis

The objective is to identify the main mechanisms and parameters establishing the HCPL robustness and stability for both configurations.

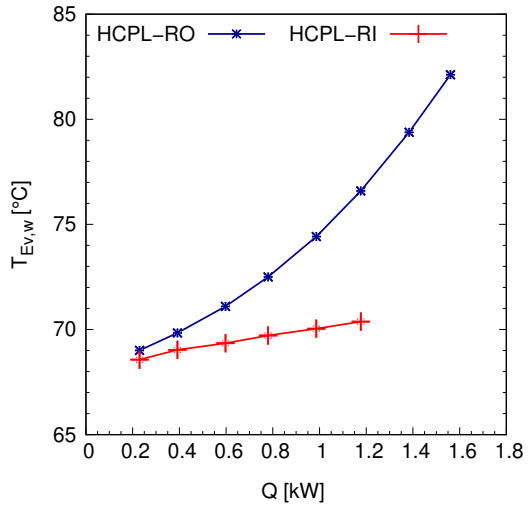

Figure 8: Comparison of the evaporator wall temperature versus the heat flux at steady-state.

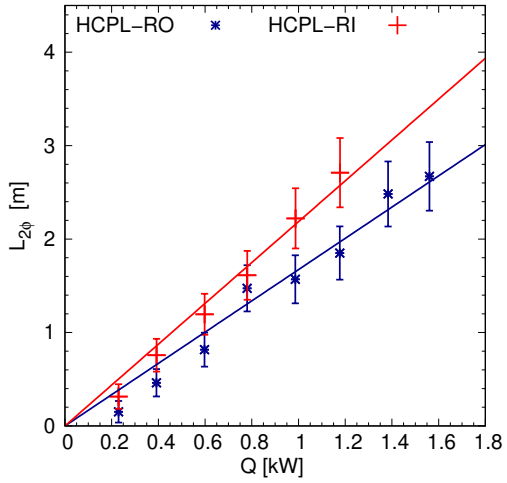

Figure 9: Comparison of the condensation length versus the heat flux at steady-state.

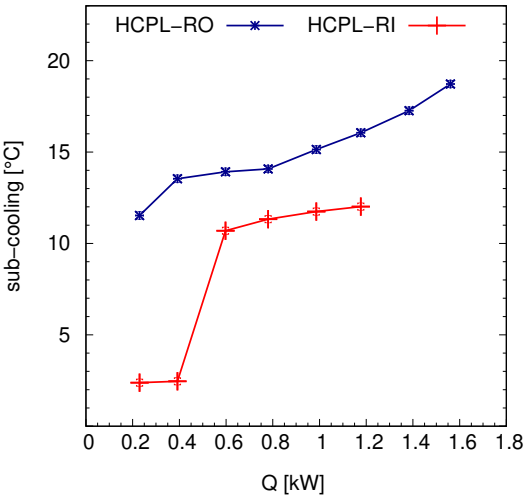

Figure 10: Comparison of the sub-cooling at the evaporator inlet versus the heat flux at steady-state.

4.1. A fundamental transient model

The approach consists in modeling only the necessary mechanisms determining the transient regime of both architectures. It is based on previous modeling efforts of the CPL dynamics [16]. Here, the reservoir is assumed to be perfectly well controlled. Moreover, the fluid flow inertia is neglected. Finally, the basic idea is that the HCPL response consecutive to a heat load change at the evaporator results from (i) the thermal inertia of solid walls at the evaporator, (ii) the mass and heat transfer in the condensation zone, (iii) the pump-controller set dynamics.

The evaporator wall is a simple capacitance MC at temperature $T_{Ev,w}$ in contact with the vaporization interface at T_V:

$$MC\frac{dT_{Ev,w}}{dt} = Q(t) - G\left(T_{Ev,w} - T_V\right) \tag{2}$$

At the condenser, the two-phase flow is assumed to be at an uniform saturation temperature $T_{C,sat}$. Then, the main hypothesis consists in assuming that a transient change of the vapor flow rate at the condenser inlet mainly modifies the length of the condensation zone $L_{2\varphi}$ i.e. the transient has negligible effect on the flow pattern. Considering a constant mean void fraction α, the mass balance of the condensation zone leads to:

$$\frac{dL_{2\varphi}}{dt} = \frac{m_{\ell\ell} - m_v}{(\rho_\ell - \rho_v)\,\alpha A_c} \tag{3}$$

The heat transfer due to the condensation is affected by the dynamic of the temperature difference between the condensation zone and the wall temperature. Introducing $h_{C,i}$ the internal heat transfer coefficient between the fluid and the wall, the energy balance on the condensation zone leads to:

$$h_{C,i}\pi D_{C,i}L_{2\varphi}\left(T_{C,sat} - T_{C,w}\right) = \Delta H_{vap}\left[m_v - \rho_v\frac{m_{\ell\ell} - m_v}{\rho_\ell - \rho_v}\right] \tag{4}$$

The wall temperature inertia is introduced for the condensation zone:

$$\frac{dT_{C,w}}{dt} = \frac{h_{C,i}\pi D_{C,i}\left(T_{C,sat} - T_{C,w}\right)}{\rho_w\, c_w\, A_{C,w}} - \frac{h_{C,o}\pi D_{C,o}\left(T_{C,w} - T_{sink}\right)}{\rho_w\, c_w\, A_{C,w}} \tag{5}$$

with $A_{C,w} = \frac{\pi}{4}\left(D_{C,o}^2 - D_{C,i}^2\right)$ and $h_{C,o}$ the total heat transfer coefficient between the wall and the heat sink.

A set of the closure equations for the two-phase loop model is given by the following relations:

- the vapor mass flow rate depends on the heat reaching the interface:

$$m_v = \frac{G\left(T_{Ev,w} - T_V\right)}{\Delta H_{vap}} \tag{6}$$

- the vaporization temperature is related to the saturation temperature in the condensation zone and to the frictional pressure losses in the vapor line and evaporator grooves assuming a linear form of the Clausius-Clapeyron equation:

$$T_V \simeq T_{C,sat} + \frac{\Delta p_V + \Delta p_{V,gr}}{\frac{dp_{sat}}{dT}} \tag{7}$$

- in a similar way, the momentum balance on the liquid between the condenser and the reservoir inlet leads to:

$$T_{C,sat} \simeq T_{R,sat} + \frac{\Delta p_R + \Delta p_{C\to R} + \rho_\ell g Z_R - \Delta p_{pump}}{\frac{dp_{sat}}{dT}} \quad (8)$$

The centrifugal pump pressure head is a non-linear function with the mass flow rate and the rotational speed:

$$\Delta p_{pump} = a\, w^2 - b\, w\, m_{\ell\ell} \quad (9)$$

The rotational speed is the process variable which is controlled by a PI law:

$$w = K_p\ (\Delta p_{Ev} - \Delta p_{Ev,set}) + \frac{K_p}{\tau_I} \int_0^t (\Delta p_{Ev} - \Delta p_{Ev,set})\ d\tau \quad (10)$$

with Δp_{Ev} the corresponding evaporator pressure head previously defined in equation (1).

The set of equations (1) to (10) provides a full HCPL-RI model. The modeling of the HCPL-RO is based on the same equations excepted equations (8) and (9) which are modified as follows:

$$T_{C,sat} \simeq T_{R,sat} + \frac{\Delta p_R + \Delta p_{C\to R} + \rho_\ell g Z_R}{\frac{dp_{sat}}{dT}} \quad (11)$$

$$\Delta p_{pump} = a\, w^2 - b\, w\, m_v \quad (12)$$

The model parameters such as the evaporator global conductance and capacitance, the heat transfer coefficients at the condenser, were quantified using the experimental temperatures at steady-state. Conventional equations were used to relate the pressure losses due to the friction along the pipes with the fluid flow rate and regime. The pump parameters are $a = 7.3.10^{-5}\ Pa/rpm^2$ and $b = 90\ Pa\ s/(kg\ rpm)$.

Note that many details were deliberately removed in the model with the objective to isolate concisely what coupling is constitutive of HCPL robustness and stability. As a consequence, an accurate data simulation cannot be reached without additional modeling efforts taking into account e.g. heat conduction in the evaporator wall and in the heating tool, vaporization in the wick, transient vapor percolation within the evaporator core, wall and fluid temperatures in transport lines, reservoir dynamics, pump intrinsic dynamic, etc.

4.2. Analysis in the frequency domain

The comparison of both HCPL responses is not straightforward to perform in the time domain as delays and deviations are highly dependent on the heat load signal. A most suitable approach is based on the transfer function which gives the specific features of the dynamical linear response in the frequency domain. As the HCPL model is non-linear, the analysis is restrained to the dynamic developing close to the steady-state and consecutive to a small change in the heat load $Q^\star + \delta Q$. The HCPL model linearization is obtained using the assumption that each variable $\eta(t)$ deviates from the steady-state by a infinitely small perturbation $\delta\eta(t)$ i.e. $\eta(t) = \eta^\star + \delta\eta(t)$ with $\eta^\star$ the steady-state variable when $Q^\star$ is applied at the evaporator. Then, the transfer function $H(\omega)$ under consideration in this work is given by:

$$\widehat{\delta\Delta p}_{Ev} = H(\omega)\, \widehat{\delta Q} \quad (13)$$

where $\widehat{\delta\Delta p}_{Ev}$ and $\widehat{\delta Q}$ are the Fourier transform of the corresponding time domain variables. Then, the sensitivity of the response with the heat load can be reached by computing the modulus $|H(\omega)|$. The determination of $H(\omega)$ is detailed in Appendix A.

4.2.1. Influence of the pump location

The objective is to analyze the impact of the pump location on the HCPL dynamics by comparing the modulus $|H(\omega)|$ for both configurations. The transfer functions were estimated at $0.6\,kW$, $1\,kW$ and $1.6\,kW$ using strictly the same set of parameters. In particular, the controller coefficients were set to $K_p = 3\,rpm/Pa$ and $\tau_I = 2\,s$. As the consequence, the deviations are only due to the modification of the pump location.

Figure 11 shows the $|H(\omega)|$ magnitude responses versus the frequency. These results first confirms that the HCPL-RO is very robust to a heat load change: (i) the linear response never exceeds $1\ Pa/W$ and (ii) the robustness is reinforced by the heat load increase as the magnitude decreases with the heat load increase. For the HCPL-RI, the magnitude response becomes greater beyond $10^{-2}\ rad/s$. Moreover, the opposite behavior is observed with the heat load increase within an intermediate frequency range $[0.1\ rad/s; 1\ rad/s]$ where the magnitude starts to increase significantly. A peak value close to $40\ Pa/W$ is reached at $1.6\,kW$ for $\omega_p \sim 0.3\ rad/s$. At this point, the response ratio reaches two orders of magnitude. Actually, if a heat load step displacement is applied, it will necessarily excite this resonance leading to large deviation. Hence, consistently with the experiments behavior, the model shows that the HCPL robustness is largely affected by the pump location at the reservoir inlet.

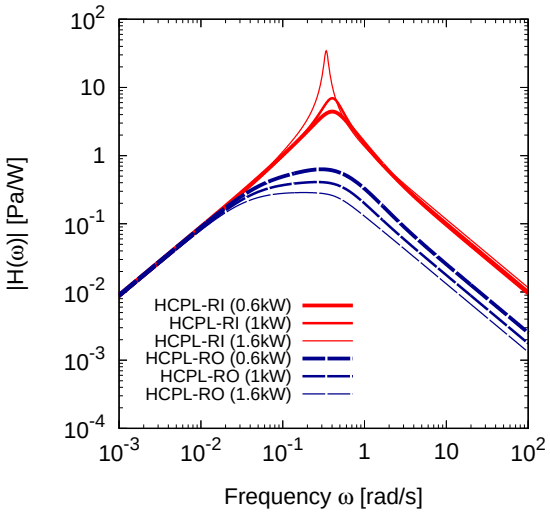

Figure 11: $|H(\omega)|$ magnitude response for both HCPL configurations and for different heat loads.

In order to understand how this behavior appears, an important information is given by the feedback approach [17]. Actually, it can be shown that the transfer function $H(\omega)$ is also given by :

$$\begin{cases} H(\omega) = S(\omega)\, G(\omega) & \text{(14a)} \\ \text{with} \quad S(\omega) = \dfrac{1}{1 + L(\omega)} & \text{(14b)} \end{cases}$$

In these equations, $G(\omega)$ is the so called open loop transfer function defined such as $\widehat{\delta\Delta p_{Ev,OFF}} = G(\omega)\,\widehat{\delta Q}$ i.e. $G(\omega)$ is the corresponding transfer function of $H(\omega)$ when the HCPL control is off (there is no more feedback between w and Δp_{Ev} so that the pump rotational speed is kept constant). The sensitivity function $S(\omega)$ is related to the feedback loop gain $L(\omega)$ which includes the effect of the PI controller. Thus, $S(\omega)$ provide an estimation of the control performance: if $|S(\omega)|$ is smaller than 1, disturbances are rejected and the regime is robust. But if not, the control will tend to transiently drive the HCPL away from the steady-state (positive feedback situation in the physicists literature) resulting in larger deviation from the set point. However, the steady-state is still reachable since $|S(\omega)|$ remains finite and moderate. This non-robust response is called fragile.

The open loop responses are shown in figure 12. Without any control, HCPL responses are very similar. Both systems behave as a low-pass filter : for frequencies lower than about $5\,10^{-2}\,rad/s$, $\widehat{\delta\Delta p_{Ev,OFF}}$ increases with the heat load as expected in the single capillary regime. Beyond that, $|G(\omega)|$ tends to zero indicating that $\widehat{\delta\Delta p_{Ev,OFF}}$ is weakly affected by high frequency perturbations. Actually, the pump location at the reservoir inlet slightly increases the bandwidth but finally, the HCPL-RI on HCPL-RO magnitude ratio remains lower than 2. This proves that it is indeed the control scheme which is leading to the HCPL-RI resonance : the feedback between the evaporator pressure head and the pump rotational speed introduces an unexpected amplification of $\widehat{\Delta p_{Ev}}$ within $[0.1\,rad/s; 1\,rad/s]$.

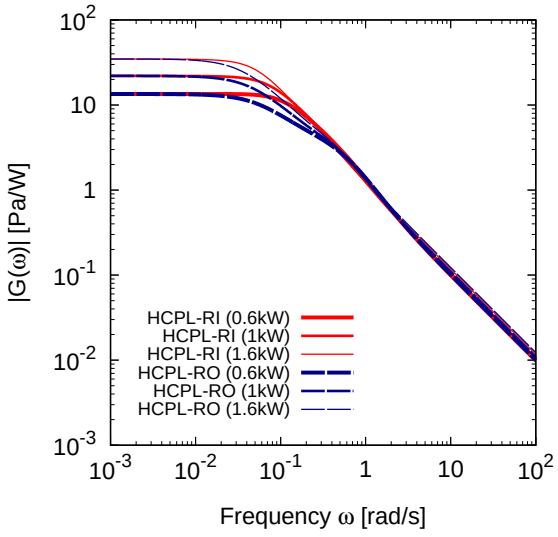

Figure 12: $|G(\omega)|$ magnitude response for both HCPL configurations and for different heat loads.

This statement is confirmed by the magnitude of the sensitivity function $|S(\omega)|$ shown in figure 13. The control loop is indeed leading to a HCPL-RI fragile response in the $[0.1\,rad/s; 1\,rad/s]$ range. The sensitivity magnitude response increases simultaneously and then, the pump actuation will cause a regime that is less and less robust as the heat load increases. The resonant peak value $|S(\omega)| \sim 10$ is reached for ω_p at $Q^\star = 1.6\,kW$. Actually, looking at the HCPL-RI maximum curve, it can be found that $|S(\omega)| \to +\infty$ as the heat load increases again. This behavior is rigorously reached since $L(\omega) = -1$ at $Q^\star \simeq 1.8\,kW$. It corresponds to a system bifurcation : the steady-state becomes unstable and any disturbance will definitively lead to growing oscillations as observed in the experiments.

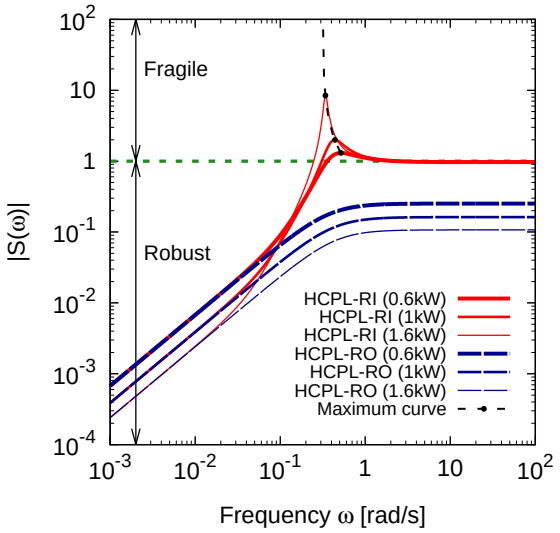

Figure 13: $|S(\omega)|$ magnitude response for both HCPL configurations and for different heat loads.

The model presented in this study is thus able to describe the general features of both HCPL responses. The influence of the pump location on the HCPL dynamics is satisfactorily estimated : the HCPL-RO robustness and its reinforcement by the the heat load increase, the HCPL-RI fragile behavior and its deterioration with the heat load increase until the manifestation of an instability. It appears now necessary to figure out which are the leading mechanism to that undesirable behavior.

4.2.2. Influence of the condenser on the HCPL-RI robustness

As mentioned before, the transient fragile response corresponds to a positive feedback behavior : an increase of Δp_{Ev} will result in a higher increase of Δp_{Ev}. According to equation (1), this could be effective in two different ways : (i) for a given Δp_{loop} variation, an increase of Δp_{Ev} is leading to a lowering of Δp_{pump}, or (ii) for a given Δp_{pump} variation, an increase of Δp_{Ev} is leading to an increase of Δp_{loop}.

In the first case, this effect could be related to the natural mass flow rate overshoot in the liquid line consecutive to a heat load increase : equation (9) shows that, if not balanced by the pump speed increase, an increase of the mass flow rate could

limit the pump pressure head. In this equation, the parameter b provides the pump ability to maintain its performance as the pump discharge rate increases. The influence of this parameter on the linear response is shown on Figure 14. On this figure, the maximum of $|S(\omega)|$ is provided at a given heat load (x-axis) and for a given b pump parameter (y-axis). The maximum is obtained by exploring the frequency range as shown in the previous figure 13. The corresponding maximum at $0.6\,kW$, $1\,kW$ and $1.6\,kW$ for $b = 90\,Pa\,s/(kg\,rpm)$ are plotted as reference on figure 14. Then, this surface plot of the $|S(\omega)|$ maximum indicates the robustness of a HCPL-RI for different b pump parameter and for a given range of operating heat load. The response also includes the linear stability analysis of the steady-state. The red broken line provides the parameters b and $Q^\star$ values when the steady-state becomes unstable. The results on figure 14 show that the unstable domain is significantly reduced by a b decrease confirming that the pump discharge rate is influencing the HCPL-RI. However, this effect does not appear to be the positive feedback cause. Actually, it is noticeable that $|S(\omega)|$ is not lower than 1 and moreover, the instability still persists at high heat load when $b = 0$.

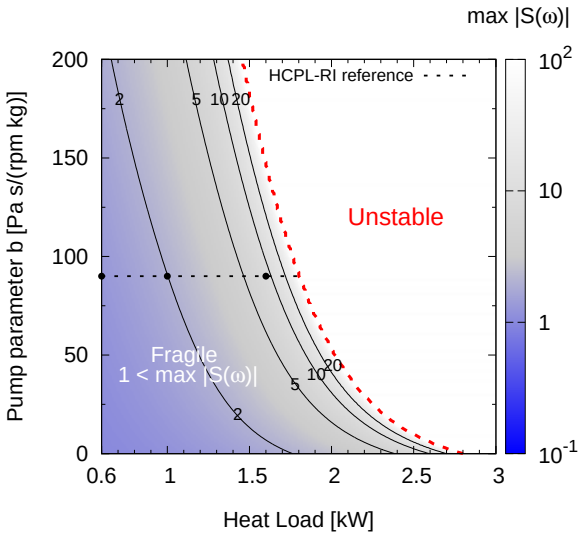

Figure 14: Surface plot of $|S(\omega)|$ magnitude maximum vs the heat load and the b pump parameter for the HCPL-RI system.

It is then necessary to understand how an increase of Δp_{Ev} could increase Δp_{loop}. Actually, when the pump pressure head increases, the pressure in the condenser falls down (see figure 2). As a consequence, the saturation temperature in the condensation zone decreases and the heat transfer with the internal condenser wall is reduced. Then, more vapor transiently flows in the condenser resulting in larger liquid discharge to the reservoir and then in a significant pressure drop increase. This analysis is consistent with the large increase of the liquid flow rate overshoot observed in the HCPL-RI experiments and it can be confirmed by the investigation of the role of the condenser. Figure 15 shows the $|S(\omega)|$ maximum for the $[0.6\,kW; 3\,kW]$ range when the external heat transfer coefficient $h_{C,o}$ is increased. In order to investigate a more representative device, a classical condenser made of stainless steal with thinner internal wall is considered in these results. A significant magnitude reduction is achieved with the heat transfer coefficient increase. Moreover, the HCPL-RI becomes robust at $h_{C,o} > 750\,W\,K^{-1}\,m^{-2}$. The unstable domain is simultaneously rejected beyond $3\,kW$. Finally, the heat load range of robustness reaches $[0.6\,kW; 1.8\,kW]$. Actually, the heat transfer coefficient increase is leading to less wall thermal inertia : the heat conduction is both faster and more intense. The condensation zone length and the two-phase front motion are then reduced so that the liquid flow rate overshoot in the liquid line is drastically limited. The pump action can be predominant among the loop pressure drop increase so that the control makes the system relaxing to the set-point. A positive feedback behavior is still occurring at high heat load. However, these results demonstrated that the resonance deteriorating the HCPL-RI robustness could be avoided within a significant range of heat load by a suitable improvement of the condenser efficiency.

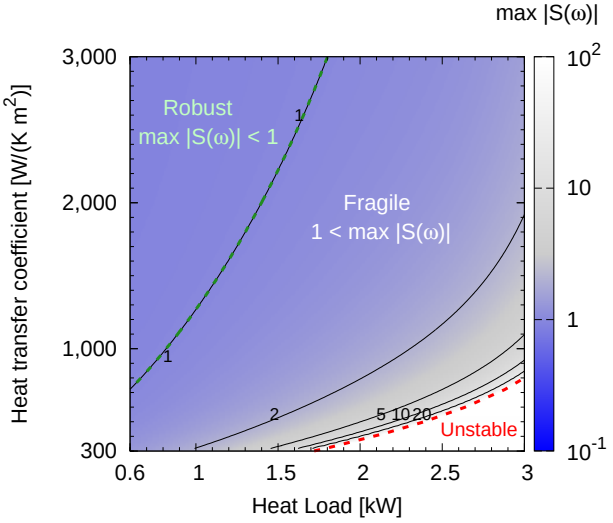

Figure 15: Surface plot of $|S(\omega)|$ magnitude maximum vs the heat load and the external heat transfer coefficient $h_{C,o}$ for the HCPL-RI system.

5. Conclusion

Capillary two-phase loops assisted with a mechanical pump were investigated and compared under the same operating conditions such that the total loop pressure losses were greater than the evaporator capillary limit. They only differ from the pump location either at the reservoir inlet or at the reservoir outlet. The results have revealed a great difference in dynamics consecutive to heat load steps :

- the HCPL-RO is robust and this regime is reinforced by the heat load increase,
- the HCPL-RI develops a more fragile regime with larger evaporator pressure deviations and larger flow rate overshoots in the liquid line. This behavior increases with the heat load until the appearance of undamped oscillations damaging for the hybrid system.

This study has also identified the effect of the pump placement on the loop temperatures and its benefit : by decreasing the pressure at the evaporator outlet, the HCPL-RI moderates the evaporator wall temperature increase; by increasing the pressure at the evaporator inlet, the HCPL-RO decreases the risks of boiling upstream the porous wick.

The model presented in this study is thus able to describe the general features of both HCPL responses.

The modeling efforts has shown that the general features of HCPL dynamics were satisfactorily captured taking into account the thermal inertia of solid walls at the evaporator, the mass and heat transfer in the condensation zone and the controller. An analysis based on the linear response in the frequency domain, enabled a quantitative HCPL dynamics comparison and demonstrated that the HCPL-RI robustness is deteriorated by a positive feedback between the pump action and the condensation dynamics. It has be shown that this behavior is leading to a system bifurcation at high heat load consistently with the experiments oscillations. However, a more efficient condenser is able to make the HCPL-RI robust for a significant range of heat loads.

This is the first condition in considering the pump assistance of LHP. However, the dynamics induced by the reservoir temperature is very specific in LHP and it could increase or decrease depending on the loop conductance mode. So it is difficult to conclude at that point if a HLHP will be robust and stable and specific study with a full model are needed.

Acknowledgment

Financial support from the IRT Saint-Exupéry is gratefully acknowledged.

Appendix A. Determination of $G(\omega)$ and $L(\omega)$

First, a linearization of equations (1) to (10) is performed. Then, a partial elimination is made leading to the following linear system based on a reduced number of variables:

$$\begin{cases} \dfrac{d}{dt}\left|\delta\eta\right\rangle = A\left|\delta\eta\right\rangle + \left|B_1\right\rangle \delta w + \left|B_2\right\rangle \delta Q & \text{(A.1a)} \\ \delta\Delta p_{Ev} = \left\langle C\right|\left.\delta\eta\right\rangle + d\,\delta w & \text{(A.1b)} \\ - - - - - - - - - - - - - - - & \\ \delta w = K_p\,\delta\Delta p_{Ev} + \dfrac{K_p}{\tau_I}\displaystyle\int_0^t \delta\Delta p_{Ev}\,d\tau & \text{(A.1c)} \end{cases}$$

where $\left|\delta\eta\right\rangle = \left|\delta T_{Ev,w}, \delta L_{2\varphi}, \delta T_{C,w}\right\rangle$ and A is a square matrix.

In the Fourier space, the preceding system becomes a set of algebraic relations:

$$\begin{cases} i\omega\left|\widehat{\delta\eta}\right\rangle = A\left|\widehat{\delta\eta}\right\rangle + \left|B_1\right\rangle \widehat{\delta w} + \left|B_2\right\rangle \widehat{\delta Q} & \text{(A.2a)} \\ \widehat{\delta\Delta p_{Ev}} = \left\langle C\right|\left.\widehat{\delta\eta}\right\rangle + d\,\widehat{\delta w} & \text{(A.2b)} \\ - - - - - - - - - - - - - - - & \\ \widehat{\delta w} = -K(\omega)\,\widehat{\delta\Delta p_{Ev}} \quad \text{with} \quad K(\omega) = -K_p + i\dfrac{K_p}{\tau_I\omega} & \text{(A.2c)} \end{cases}$$

Finally, eliminating $\left|\widehat{\delta\eta}\right\rangle$ such as $\widehat{\delta\Delta p_{Ev}} = G(\omega)\,\widehat{\delta Q}$ when $\widehat{\delta w} = 0$ and $\widehat{\delta\Delta p_{Ev}} = H(\omega)\,\widehat{\delta Q}$ when $\widehat{\delta w}$ is active, it can be shown that:

$$\begin{cases} G(\omega) = \left\langle C\right|\left(i\omega\mathbb{1} - A\right)^{-1}\left|B_2\right\rangle & \text{(A.3a)} \\ L(\omega) = K(\omega)\left[\left\langle C\right|\left(i\omega\mathbb{1} - A\right)^{-1}\left|B_1\right\rangle + d\right] & \text{(A.3b)} \end{cases}$$

Appendix B. Uncertainty determination

Data		**Uncertainty (U)**
Δp_{pump}		$116\,Pa$
Δp_{Ev}		$112\,Pa$
Δp_{loop}		$158\,Pa$
$p_{R,sat}$		$486\,Pa$
$p_{Ev,in}$		$536\,Pa$
$p_{C,in}$		$560\,Pa$
$T_{Ev,in,sat}$	methanol data from [18]	
at $63°C$, $0.9555\,bar$	$dP_{Sat}dT = 3.80\,kPa\,K^{-1}$	$0.14°C$
at $75°C$, $1.5117\,bar$	$dP_{Sat}dT = 5.55\,kPa\,K^{-1}$	$0.10°C$
$T_{C,Sat}$		
at $60°C$, $0.8470\,bar$	$dP_{Sat}dT = 3.44\,kPa\,K^{-1}$	$0.17°C$
at $70°C$, $1.2542\,bar$	$dP_{Sat}dT = 4.76\,kPa\,K^{-1}$	$0.12°C$
$m_{\ell\ell}$	$[0.1\,g/s, 0.643\,g/s]$	$1\%\,m_{\ell\ell} \le U \le 4.8\%\,m_{\ell\ell}$
	$[0.643\,g/s, 4.5\,g/s]$	$0.4\%\,m_{\ell\ell} \le U \le 1\%\,m_{\ell\ell}$
$m_{Ev,in}$	$[0.1\,g/s, 0.159\,g/s]$	$1\%\,m_{Ev,in} \le U \le 1.4\%\,m_{Ev,in}$
	$> 0.159\,g/s$	$0.3\%\,m_{Ev,in} < U < 1\%\,m_{Ev,in}$
w (speed)	at $2.721\,10^3\,rpm$	$200\,rpm$
	at $27.975\,10^3\,rpm$	$478\,rpm$
Q	total electrical power	$2.8\%\,Q$

Table B.2: Expanded uncertainty based on a coverage factor $k = 2$.

References

[1] Y. F. Maydanik, Loop heat pipes, Applied Thermal Engineering 25 (2005) 635–657.

[2] R. Schweickart, L. Ottenstein, B. Cullimore, C. Egan, D. Wolf, Testing of a controller for a hybrid capillary pumped loop thermal control system, IEEE 69 (1989).

[3] C. Park, A. Vallury, J. Zuo, Performance evaluation of pump-assisted capillary two-phase loop, ASME Journal of Thermal Science and Engineering Applications 1 (2009).

[4] M. Crepinsek, C. Park, Experimental analysis of pump-assisted and capillary-driven dual-evaporators two-phase cooling loop, Applied Thermal Engineering 38 (2012) 133–142.

[5] R. V. Bejarano, C. Park, Active flow control for cold-start performance enhancement of a pump-assisted, capillary-driven, two-phase cooling loop, International Journal of Heat and Mass Transfer 78 (2014) 408–415.

[6] M. Lee, C. Park, Mechanical-capillary-driven two-phase loop: Feedback control for thin-film evaporation and capillary limit enhancement, Applied Thermal Engineering 204 (2022) 117960.

[7] C. Jiang, Z. Liu, D. Wang, J. Yang, H. Wang, J. Li, W. Liu, Effect of liquid charging process on the operational characteristics of pump-assisted capillary phase change loop, Applied Thermal Engineering 91 (2015) 953–962.

[8] C. Jiang, W. Liu, H. C. Wang, D. D. Wang, J. G. Yang, J. Y. Li, Z. C. Liu, Experimental investigation of pump-assisted capillary phase change loop, Applied Thermal Engineering 71 (2014) 581–588.

[9] H. Zhang, C. Jiang, Z. Zhang, Z. Liu, X. Luo, W. Liu, A study on thermal performance of a pump-assisted loop heat pipe with ammonia as working fluid, Applied Thermal Engineering 175 (2020) 115342.

[10] I. Setyawan, N. Putra, I. I. Hakim, Experimental investigation of the operating characteristics of a hybrid loop heat pipe using pump assistance, Applied Thermal Engineering 130 (2018) 10–16.
[11] M. Levêque, S. Dutour, J. Lluc, P. Lavieille, M. Miscevic, Y. Bertin, R. Mari, L. Fourgeaud, Experimental study of a Capillary Pumped Loop assisted with a mechanical pump placed at the evaporator inlet, Applied Thermal Engineering 169 (2020).
[12] V. Ayel, L. Lachassagne, Y. Bertin, C. Romestant, D. Lossouarn, Experimental Analysis of a Capillary Pumped Loop for Terrestrial Application, Journal of Thermophysics and Heat Transfer 25 (2011) 561–571.
[13] V. Dupont, S. Van Oost, L. Barremaecker, Increasing the CPL power at startup by using a check valve, in: Proceedings of the 16th International Heat Pipes Conference (IHPC) 2012, 2012, pp. 249–254. 16th International Heat Pipe Conference (16th IHPC), Lyon, France, May 20-24, 2012.
[14] F. Accorinti, V. Ayel, Y. Bertin, Steady-state analysis of a Capillary Pumped Loop for Terrestrial Application with methanol and ethanol as working fluids, International Journal of Thermal Sciences 137 (2019) 571–583.
[15] A. Kaled, S. Dutour, V. Platel, J. Lluc, Experimental study of a Capillary Pumped Loop for cooling power electronics: Response to high amplitude heat load steps, Applied Thermal Engineering 89 (2015) 169–179.
[16] S. Dutour, A. Kaled, Analytical and numerical results for the dynamics of capillary pumped loops and loop heat pipes subjected to high amplitude heat load steps, Applied Thermal Engineering 126 (2017) 1107–1114.
[17] J. Bechhoefer, Feedback for physicists: A tutorial essay on control, Rev. Mod. Phys. 77 (2005) 783–836.
[18] D. Ambrose, C. Sprake, Thermodynamic properties of organic oxygen compounds xxv. vapour pressures and normal boiling temperatures of aliphatic alcohols, The Journal of Chemical Thermodynamics 2 (1970) 631–645.